JOURNAL OF SPACECRAFT AND ROCKETS
Vol. 32, No. 2, March–April 1995

Selenopotential Field Effects on Lunar Landing Accuracy

Dan G. Tuckness*
University of Texas at Arlington, Arlington, Texas 76019-0018

Various gravity field models are reviewed and their influence on the amount of ΔV required for a precision landing is investigated. The effect of the models on navigation of a lunar lander, using a precision navigation scenario, is introduced. An altitude navigation sensor, using an extended Kalman filter, is established as the external updating sensor in order to improve on the uncertainty in the gravity model. The J_2 term of the lunar potential model is the dominant term, and most of the models agree on the value of its coefficient. However, the discrepancy between the models grows as the order of the harmonics increases. Simulation results show that a refined lunar potential model would increase landing target accuracy, thereby reducing guidance uncertainty and requiring less ΔV; however, the difference between the various models appears to have only a small effect on the ΔV required.

Nomenclature

$\boldsymbol{A}$ = state gradient matrix
$\boldsymbol{G}$ = sensor model vector
$\boldsymbol{H}$ = observation update matrix
$\boldsymbol{K}$ = Kalman-filter gain vector
$\boldsymbol{P}$ = covariance matrix after navigation update
$\bar{\boldsymbol{P}}$ = covariance matrix before navigation update
$\boldsymbol{Q}$ = state noise matrix
$\boldsymbol{R}$ = navigation measurement noise matrix
$\boldsymbol{W}$ = weighting matrix (identity matrix for this study)
$\boldsymbol{X}$ = state vector
Φ = state transition matrix

Introduction

LACK of an adequate lunar gravity model affects two essential navigation problems for a spacecraft, namely, determining the position of the spacecraft at a specified time (orbit determination) and predicting the future course of the spacecraft (trajectory prediction). These problems have a direct influence on the accuracy of a lunar landing spacecraft, especially when landing at a preselected point on the surface. Such a landing is generally termed a "precision landing" and is defined in terms of a landing area within a specified radius from the preselected point.[1–3] For the Common Lunar Lander (CLL) the specified radius is 5 km. This paper investigates the influence of various lunar gravity models on a precision lunar landing.

Lunar Gravity Model

The gravitational potential of the moon is usually represented as an expansion in spherical harmonics. Using this representation, researchers have been processing the lunar-orbit data to obtain improved models of lunar gravity. The inability to model the lunar gravitational field mathematically was observed for the first time during the Lunar Orbiter I mission in August 1966. The Lunar Orbiter I Doppler tracking data displayed large, unexplained accelerations in the vicinity of perilune. These accelerations were larger by several orders of magnitude than those predicted from modeling errors and tracking-data noise. Considering the accuracy of the data provided by the Doppler-shift method, the uncertainties in the various gravity models used to compute the state vectors amount to a serious loss in precision.

A variety of researchers have been investigating the idea of constructing a better lunar gravity model. These include, but are not limited to, Muller and Sjogren,[4] Wong et al.,[5] Michael and Blackshear,[6] Lorrell,[7] Liu and Lang,[8] Ferrari and Ananda,[9–11] and Sagitov et al.[12] It should be noted that none of the lunar gravity models provide a complete mathematical field, primarily because of a lack of lunar far-side data.

The effects of nine different lunar gravity models (from the authors mentioned above) on the trajectory of the CLL landing vehicle were investigated. The nine models were selected for the differences in how they evolved and were constructed. An in-depth description and comparison of the models are given in Ref. 13.

Arteimis (CLL) Lander Reference Mission Scenario

The primary responsibility of the Science Exploration Initiative (SEI) is to investigate the steps required for human exploration of the Moon and Mars. One of the first steps towards human exploration will be the development robotic science missions. The purpose of the robotic missions will be to gather scientific data prior to a manned landing, and later to assist manned exploration.[14] In response to this SEI initiative, the Arteimis [or Common Lunar Lander (CLL)] program was established with NASA–Johnson Space Center (JSC) as the lead center. The Arteimis Program includes rapid, near-term development of a variety of small experimental and operational payloads, provides a low-cost capability to deliver these payloads to any location on the lunar surface, and supports the analysis of the data returned.

The CLL navigation accuracy requirements considered in this study specify a landing target accuracy of 5 km (3σ); other future SEI missions, such as the manned Mars missions, have requirements of landing autonomously with a target accuracy of 10 m (3σ). The CLL would arrive at the moon in approximately 4–5 days (minimum-energy translunar trajectory) and would be placed in a 100-km circular lunar parking orbit.[15] The parking-orbit inclination is dependent upon landing-site selection and will be determined at a later date. Potential landing sites range from the Oriental Basin (53°S, 79°W) to the Nectaris Basin (35°S, 42°E).[16] An inclination of 30 deg was selected, since it is between the special cases of a 0-deg inclination (equatorial orbit) and the 67-deg critical inclination. It should be noted that results obtained are dependent upon the orbital inclination and landing/deorbit positions with respect to the surface. Therefore, the trends of the gravitational influence on the trajectory of the CLL lander should be considered instead of the exact solution, unless the orbit of interest has a 30-deg inclination.

Once the landing area is selected and it is time to deorbit for landing, a ΔV burn of 23.0 m/s is performed to establish the deorbit trajectory. About 16 km from the touchdown point, the landing jets are ignited and a propulsive landing is performed during the terminal phase. For this study, the terminal guidance algorithm consisted of a derivative of the explicit guidance (E guidance).[17] Basically, it solves a two-point boundary-value problem constraining the downrange change in acceleration, given the initial and terminal conditions.

Table 1 gives a possible timeline of the descent and landing. The mass of the CLL is approximately 1350 kg. The propulsive

Received Sept. 17, 1993; revision received Jan. 17, 1994; accepted for publication May 13, 1994.

*Assistant Professor, Department of Mechanical and Aerospace Engineering, Box 18018. Member AIAA.

landing show in Fig. 1 requires approximately 1855-m/s ΔV with a maximum T/W ratio of 2.0 (Earth g).

The following integrator models and initial conditions were used to simulate the trajectories used in this study:

1) Numerical integration of the state vector was performed using a fourth-order Runge–Kutta integrator with a fixed stepsize of 1.0 s.

2) Initial orbital elements:

a) Semimajor axis: 1787.53 km.

b) Eccentricity: 0.027971558.

c) Inclination: 30.0 deg.

d) Argument of perilune: 0.0 deg.

e) Longitude of ascending node: 0.0 deg.

f) Time to perilune: 3390.8 s.

3) Lunar equatorial radius: 1737.53 km.

4) Lunar rotation rate: 2.6621916×10^{-6} rad/s.

5) Gravitational constant: The gravitational constants of the various models range from 4902.78 to 4902.8 km^3/s^2. Because the different gravitational constants result in different orbits for a given state vector, investigation of the influence of the gravitational parameter values was undertaken. Using the two-body energy equation, energy = −(gravitational parameter)/(2 × semimajor axis), the gravitational parameter becomes directly proportional to differences in the semimajor axis. Varying the gravitational parameter by $4902.8 - 4902.78 = 0.02$ km^3/s^2 and holding the energy constant results in a 2 ± 20-m difference in the semimajor axis. Because the errors found using the various gravity models are on the order of hundreds of kilometers, this difference is well within the accuracy limitations of this study.

Table 1 CLL descent and entry timeline

		h:min:s
CLL tracked by DSN while quiescent		−24:00:00
Initial state and navigation covariance uplinked from DSN		−02:00:00
Align lander IMU using star tracker		0:00:00
Deorbit phase		
Deorbit burn	ΔV = 23.0 m/s	0:00:00
Terminal phase		
Terminal descent engines active	alt. = 16 km	0:42:00
Landing		0:59:00

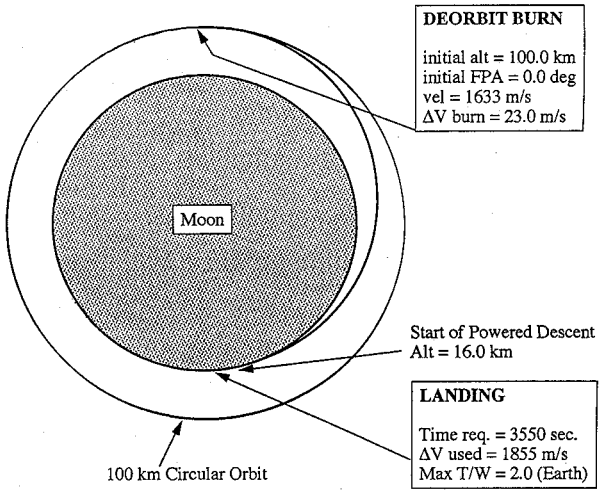

Fig. 1 CLL landing navigation scenario.

Gravity Field Effects on Lunar Landing Trajectories

A comparison was made between the changes in the orbital elements, the terminal target miss distance (without the use of a terminal guidance), and the ΔV requirement for a guided precision landing using the aforementioned lunar potential models. A deorbit-through-touchdown simulation was used, and the initial conditions for the trajectory are given at the beginning of this paper. For simplicity and a better understanding of the influence of each of the models, the initial position of the vehicle in inertial space was assumed to be known.

Nine models (cases 1 through 9) were investigated, and their various orbital elements were compared with those of the nominal case (inverse square law only). The deviations in the orbital elements result in a terminal target (or landing-point) miss distance. Because most guidance methods depend on linearized equations, the unguided miss distance (terminal target miss distance) can provide information on how far away from the reference trajectory the guidance algorithm may need to function. This results in a measure of guidance accuracy limitations. It also gives an indication of how much thrusting is required to remain on the reference trajectory. Therefore, the unguided miss distance is a measure of how much work the terminal guidance must do in order to remain on the reference trajectory or land at a preselected specific point on the surface. Table 2 gives the deviations in the various orbital elements upon reaching the terminal-landing-point altitude. The perturbation of the semimajor axis varied from +83 to −577 m, resulting in a 660-m spread among the nine models investigated. A spread of 0.000417 was found in the values of the eccentricities. The processing of the longitude of the ascending node is the dominant influence in the changing of the time to periapsis and is a strong function of the oblateness coefficient J_2. Fortunately, most of the nine models agree on J_2 (with the exception of Liu's model), resulting in a spread in the maximum time to periapsis of approximately 78 s. Therefore, the time-to-go (T_{go}) estimates for the descent and landing guidance (assuming they result from a time-based terminal boundary condition, as in the E guidance used in this study and explained later in the paper) will remain fairly constant using any of the models, including the lower-order models that are more practical for on-board navigation computers.

It should be noted that Liu's model resulted in a trajectory that never reached the surface and had the largest deviation in the argument of periapsis. Altitude (or radial) errors are a consequence of deviations in the orbital eccentricity and argument of periapsis. In an attempt to construct a global lunar gravity map that included

Table 2 Deviations in terminal orbital elements for various gravity models

	Unperturbed values					
	a, km	e	i, deg	ω, deg	Ω, deg	t_p, s
	1787.530	0.0279721	30.000	0.000	0.0000	0.000
	Deviations					
Case	Δa, km	Δe	Δi, deg	$\Delta\omega$, deg	$\Delta\Omega$, deg	Δt_p, s
1 (Sjogren)	−0.080	0.000704	−0.012	−0.226	−0.0404	243.686
2 (Wong)	0.040	0.000591	−1.043	−0.911	−0.0266	211.253
3 (Michael)	−0.038	0.000958	−0.005	−0.713	7.3677	273.550
4 (JPL1)	−0.577	0.000541	−0.001	−0.341	−0.0733	260.646
5 (JPL2)	0.083	0.000545	−0.014	0.375	−0.0425	201.198
6 (Liu)[a]	−0.162	0.000572	−0.028	−1.140	0.0634	0.112
7 (Ferrari 77)	−0.208	0.000847	−0.013	0.162	−0.0414	274.509
8 (Ferrari 79)	−0.470	0.000741	−0.010	0.047	−0.0383	278.283
9 (Sagitov)	−0.360	0.000800	−0.011	0.041	−0.0396	278.067

[a]Lowest altitude obtained = 0.863 km.

Table 3 Target miss distance for various gravity models

Case	Model (order)	North error, km	East error, km
0	Nominal	0.000	0.000
1	Sjogren (3 × 3)	359.392	−201.491
2	Wong (16 × 16)	332.654	−187.234
3	Michael (6 × 6)	420.831	−233.628
4	JPL 1 (4 × 4 + 4)	388.424	−216.316
5	JPL 2 (4 × 4 + 4)	300.158	−169.610
6	Liu (8 × 8 + 7)	34.958[a]	−21.343[a]
7	Ferrari 77 (16 × 16)	403.482	−224.539
8	Ferrari 79 (16 × 16)	402.355	−224.034
9	Sagitov (16 × 16)	405.769	−225.770

[a]Lowest altitude obtained = 0.863 km.

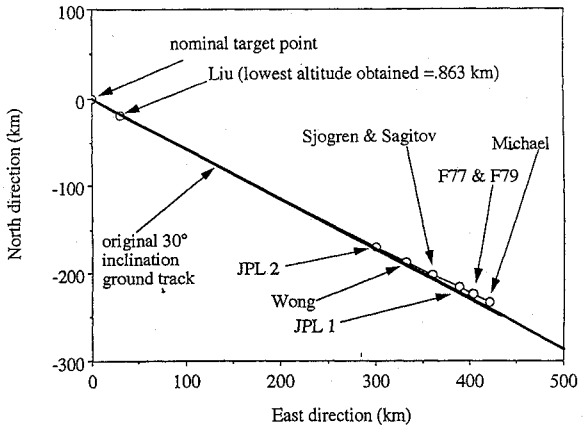

Fig. 2 Surface impact points using various gravity field models.

both the near- and far-side features, Liu processed short- and long-arc data trajectories together. This resulted in a lunar gravity field with unique characteristics that differ from those of the other gravity models, which are constructed of either the long- or the short-arc trajectories processed separately. References 13 and 17 offer an in-depth investigation of the correlation, method of processing, and influence of the various lunar potential models used in this study.

Crossrange errors result from deviations in the orbital inclination and the longitude of the ascending node. Using Michael's model results in the largest deviation in the longitude of ascending node and eccentricity, which in turn results in the largest north and east deviations. Transforming the north and east deviations into downrange and crossrange error, Michael's model results in the largest downrange and crossrange deviation. This is shown in Fig. 2. A periodic downrange error, with a period of one revolution, results from the error in predicting the orbital eccentricity. This error is of the form $EV = t \sin \omega t$ (where EV is the downrange error, t is time, and ω is the orbital mean motion); thus, the error amplitude increases with time. A secular downrange error is introduced by errors in the local determination of the semimajor axis. For a precision landing, the exact terminal target position is known a priori and the vehicle is required to land as close as possible to that point. This results in increased fuel cost if the landing target is missed. Because all missions are limited in the amount of maneuvering fuel they are allotted, and carrying excess terminal maneuvering fuel can substantially drive up mission cost, minimization of maneuver fuel usage is essential. Table 3 gives the topographical north and east miss distances with respect to an a priori landing site that was established using the nominal (or unperturbed) trajectory without guidance (free fall). The nominal case is an inverse square law only: Sjogren is a 3 × 3 model, Michael a 6 × 6, JPL1 a 4 × 4 with zonal harmonics up to 8, JPL2 has the same order as JPL1, Liu is an 8 × 8 with zonal harmonics up to degree 15, and all others are full 16 × 16 models. All cases (except for Liu) were terminated at surface impact. Liu's model was not terminated at the surface, because in it the CLL vehicle never reaches the surface.

In order to estimate the cost of the miss distances given in Table 3, a guidance algorithm was implemented to find the total ΔV required to land at the precision landing site. It should be noted that this investigation is for comparison only. The E guidance used in this study is not an optimized guidance. Therefore, the amount of required ΔV may differ from other guidance methods. Table 4 shows the ΔV requirements for various orders of the gravity models. The nominal model required 1855 m/s of ΔV. From Table 4 one can see that influence of the coefficient J_2 contributes most of the additional ΔV required. For some models there was very little difference in the amount of ΔV required between the 6 × 6 and 16 × 16 models.

Landing Navigation Error Analysis

A covariance analysis was performed to estimate the navigation errors resulting from errors in the the lunar gravity field model. Two different types of navigation methods (with and without secondary navigation systems) were investigated for the Liu, F77, and Sagitov gravity models. The primary CLL navigation system was assumed to consist of an inertial measurement unit (IMU, the primary navigation system), a Deep-Space Network (DSN) transponder, and a star tracker. The DSN transponder is only used to provide the initial position fix (or trajectory uncertainty), and the star tracker is only used to align the IMU. The secondary navigation method consisted of a radar altimeter. It was assumed that the primary sensor (IMU) would be used throughout the entire mission, whereas the secondary sensor would be used to aid in removing positional and attitude errors accumulated in the primary sensor. The radar altimeter measurements are processed (when available) using a full-state extended sequential Kalman filter to obtain the minimum error covariance, thereby reducing the state error. It should be noted that a full-state filter is not realistic for onboard implementation, and a suboptimal (reduced order) filter will probably be required on account of on-board processing times and memory restrictions. Therefore, only 6 × 6 gravity fields were considered for the navigation analysis.

Initial Conditions Used in Navigation Analysis

The initial covariance is based upon estimated DSN capabilities and is given in Table 5.[15] It is depicted as an upper triangular matrix with standard deviations on the diagonal and cross-correlation coefficients off the diagonal. Only the dominant cross-correlation terms (parameters correlated with the flight-path angle) were considered. The state elements are considered in a vehicle-centered coordinate system described as follows:

1) The DR (downrange) axis is in the direction of the vehicle velocity vector projected onto the local horizontal.

2) The Alt (altitude) axis is in the direction from the center of the lunar sphere to the vehicle.

3) The CR (crossrange) axis is perpendicular to both the DR and Alt axes.

Initial navigation errors used in the navigation simulation models are given in Table 6. The error model of the IMU is based on a 13XX series laser inertial navigation system (LINS). One of the primary drivers in navigation error accumulation is in large IMU misalignments incurred as a result of gyro drift. Clearly, an IMU realignment prior to entry interface is desirable, and it is assumed for this study that the lander IMU is aligned prior to separation.

For the first part of this investigation an unaided covariance analysis (no navigation updates) was performed using the three models. The creators of each of the gravity models also calculated the standard deviation of their various coefficients (including the cross-correlation coefficients) as they processed the lunar trajectory data. These were used as the initial (1σ) covariance parameters for the gravity terms.

Table 7 depicts the terminal landing (3σ) position and velocity errors found by propagating the initial standard deviations in covariance-matrix form. The 8 × 8 + 7 gravity model, by Liu, results in the worst navigation errors, with root sum squared (RSS) errors of approximately 33 km (3σ). This large error far exceeds the CLL mission navigation accuracy requirements of 5 km (3σ). Using the F77 model resulted in an RSS error of approximately 24 km (3σ), and using the Sagitov model resulted in an error of approximately 20 km (3σ). Even though much smaller results were obtained

Table 4 ΔV requirements of precision landing for various gravity models

Case	Model	ΔV required (order)		
		J_2 only	Lower order	Higher order
0	Nominal (1855 m/s)	N/A	N/A	N/A
1	Sjogren	1872	1885 (3 × 3)	N/A
2	Wong	1868	1879 (6 × 6)	1882 (16 × 16)
3	Michael	1872	1903 (6 × 6)	N/A
4	JPL 1	1872	1890 (4 × 4 + 4)	N/A
5	JPL 2	1872	1880 (4 × 4 + 4)	N/A
6	Liu	1872	1865 (6 × 6)	1870 (8 × 8 + 7)
7	Ferrari 77 (F77)	1871	1894 (6 × 6)	1897 (16 × 16)
8	Ferrari 79 (F79)	1872	1886 (6 × 6)	1887 (16 × 16)
9	Sagitov	1872	1886 (6 × 6)	1900 (16 × 16)

Table 5 Initial covariance matrix for CLL lander (1σ)

Alt, m	DR, m	CR, m	DR rate, m/s	CR rate, m/s	Alt rate, m/s
50.000	0.0000	0.0000	0.0000	−0.9990	0.0000
	200.0000	0.0000	−0.9990	0.0000	0.0000
		50.0000	0.0000	0.0000	0.0000
			0.2000	0.0000	0.0000
				0.0400	0.0000
					0.0300

Table 6 IMU and external sensor error models (1σ)[a]

Accelerometer error (H-750 LINS stapdown IMU type):	
3-axis—misalignment (Alt, DR, CR), rad	7.59E − 04, 7.59E − 04, 7.59E − 04
3-axis—bias (Alt, DR, CR), m/s^2	1.00E − 05, 1.00E − 05, 1.00E − 05
3-axis—scale factor (Alt, DR, CR), ppm	70, 70, 70
Sensor measurement error:	
Radar altimeter measurement bias, m	30.0
Radar altimeter measurement white noise, m	5.0
Unmodeled noise:	
3-axis—unmodeled system acceleration white noise, m/s^2	5.0E−08

[a]Reference 15.

Table 7 Landing position and velocity errors (3σ)

	Alt, km	DR, km	CR, km	Alt rate, km/s	DR rate, km/s	CR rate, km/s
Liu	11.124	31.525	1.567	0.02754	0.00886	0.00321
Ferrari 77	8.627	22.440	1.199	0.02189	0.00718	0.00304
Sagitor	8.655	17.712	0.937	0.01784	0.00445	0.00189

than that of Liu, both of these models also exceeded limitations. From this it is seen that in order to meet landing navigation accuracy some form of external measurement is required. The RSS velocity errors range from 18 up to 99 m/s (3σ). This amount of uncertainty during landing could lead to the destruction of most landers by exceeding the structural limitations upon impact. However, the CLL will probably contain a descent landing radar altimeter to remove this error.

The second part of this investigation studied the ability of external measurements to remove the additional errors introduce by the gravity models. The on-board radar-altimeter secondary navigation system took measurements every 10 s, starting at 60-km altitude; these were processed through an extended Kalman filter (EKF) to estimate the "cloud of uncertainty" (covariance) surrounding the state vector and aid in removing this navigation uncertainty. The mathematical model and flow of the EKF is as follows:

1) Compute the partial derivatives of the equations of motion with respect to the state variables using a central difference scheme:

$$A(t) = \frac{\partial F(X, t)}{\partial X}$$

2) Compute the time derivative of the state vector and the state transition matrix:

$$\dot{X} = f(X, T)$$

$$\dot{\Phi} = A\Phi$$

3) Integrate the state vector and the state transition matrix from time t_n to time t_{n+1} using a fourth-order Runge–Kutta integrator with a fixed stepsize of 1.0 s:

$$X = \int \dot{X}\, dt$$

$$\Phi = \int \dot{\Phi}\, dt$$

4) Propagate the covariance matrix:

$$P = \Phi \quad \bar{P} \quad \Phi^T + Q$$

5) Compute the observation update matrix:

$$H = \frac{\partial G(X, t)}{\partial X}$$

6) Compute the Kalman-filter gain using the observation update matrix:

$$K = \bar{P} \quad H^T (H \quad \bar{P} \quad H^T + R)^{-1}$$

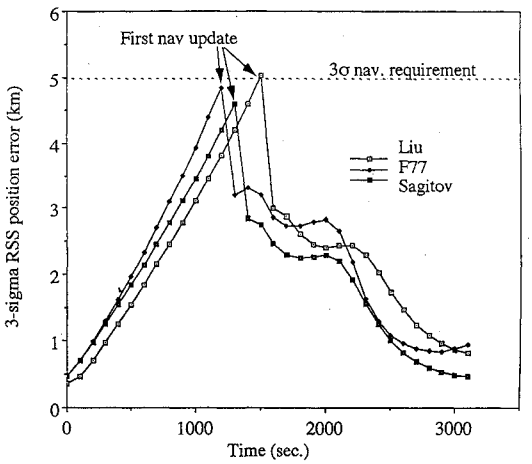

Fig. 3 3σ RSS position errors vs time.

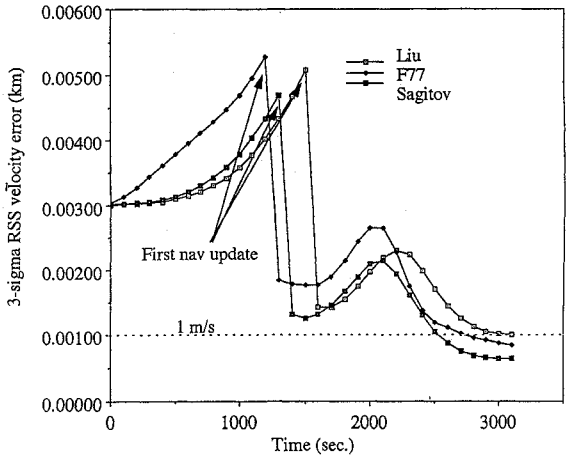

Fig. 4 3σ RSS velocity errors vs time.

7) Update the covariance matrix using the navigation Kalman-filter gain:

$$\boldsymbol{P} = (\boldsymbol{I} - \boldsymbol{W}\ \boldsymbol{K}\ \boldsymbol{H})\bar{\boldsymbol{P}}\,(\boldsymbol{I} - \boldsymbol{W}\ \boldsymbol{K}\ \boldsymbol{H})^T + \boldsymbol{W}\ \boldsymbol{K}\ \boldsymbol{R}\ \boldsymbol{K}^T$$

8) Set $\bar{\boldsymbol{P}} = \boldsymbol{P}$ for the next iteration.

9) Print results.

10) Go back to 1) for the next step in integration.

The same three gravity field models and initial conditions above were used. Figures 3 and 4 show the RSS position and velocity errors for each of the three models investigated. Note that all the gravity models resulted in reduced terminal errors when using an external measurement, which indicates that the use of an altimeter as an external update sensor could successfully reduce the uncertainty caused by error in the coefficients of the lunar potential model. Figure 3 shows that all the gravity models resulted in RSS position no greater that 2.0 km. This is well within the 5.0-km CLL mission requirement. Figure 4 shows that the three gravity models resulted in RSS velocity errors within 1.0 m/s. Most lander designs should be capable of tolerating this type of surface impact.

Conclusions

Even the best currently available lunar potential models leave much to be desired in terms of ability to describe lunar lander trajectories properly and to predict their behavior. Lack of lunar far-side data has been the major problem in determining the potential function. However, most of the models available today tend to agree on a common trend in how the lunar potential field affects a lunar trajectory. Although a refined lunar potential model would increase landing target accuracy, thereby reducing guidance uncertainty and requiring less ΔV, the difference between the various models has only a small effect on the ΔV required. The ΔV required for a terminal landing using the various models results in a 45-m/s ΔV differential (including the inverse square model). This small differential is a result of the J_2 influence being the dominant term in the gravity perturbations, and most of the models agree on the value of this coefficient. A ΔV range of 1868 to 1900 m/s was found for all models, including reduced-order models that included only the coefficient J_2. Therefore, the guidance does not appear to be severely affected by the selection of the on-board gravity model or its order, so long as it contains the J_2 term, when using the total amount of ΔV required as a performance measure.

In the investigation of the navigation error, large uncertainties were found when using Liu's gravity model and the associate standard deviations of the coefficients. The other two models investigated (F77 and Sagitov) had smaller navigation uncertainties but still exceed mission requirements without the use of external measurements. The investigation of using a radar altimeter to help in removing the navigation uncertainty demonstrated that Liu's gravity model resulted in larger terminal navigation uncertainties than the F77 or Sagitov gravity models but still met mission requirements.

References

[1]Draper, R. F., "The Mariner Mars 11 Program," AIAA Paper 88-0067, Jan. 1988.

[2]Bourke, R. D., Kwok, J. H., and Friedlander, A., "Mars Rover Sample Return Mission," AIAA Paper 89-0417, Jan. 1989.

[3]Carter, P. H., and Smith, R. S., "Mars Rover Sample Return Lander Performance," AIAA Paper 89-0633, Jan. 1989.

[4]Muller, P., and Sjogren, W., "Mascons: Lunar Mass Concentrations," *Science*, Vol. 161, No. 3842, 1968, pp. 680–684.

[5]Wong, L., Buechler, G., and Doens, W., "A Surface-Layer Representation of the Lunar Gravity Field," *Journal of Geophysical Research*, Vol. 76, No. 26, 1971, pp. 6220–6236.

[6]Michael, W., and Blackshear, W., "Recent Results on the Mass, Gravity Field & Moments of Inertia of the Moon," *The Moon*, Vol. 3, 1972, pp. 388–402.

[7]Lorell, J., "Lunar Orbiter Gravity Analysis," *The Moon*, Vol. 1, 1970, pp. 190–231.

[8]Liu, A., and Laing, P., "Lunar Gravity Analysis from Long-Term Effects," *Science*, Vol. 173, No. 4001, 1971, pp. 1017–1020.

[9]Ferrari, A., "Lunar Gravity, The First Farside Map," *Science*, Vol. 188, No. 4195, 1975, pp. 1297–1300.

[10]Ferrari, A., "Lunar Gravity, a Harmonic Analysis," *Journal of Geophysical Research*, Vol. 82, No. 20, 1977, pp. 3065–3084.

[11]Ferrari, A. and Ananda, M., "Lunar Gravity, Long-Term Keplerian Rate Method," *Journal of Geophysical Research*, Vol. 82, No. 20, July 1977, pp. 3085–3097.

[12]Sagitov, M. U., Bodri, B., Nazarenko, V. S., and Tadzhodinoz, Kh. G., *Lunar Gravimetry*, Academic, New York, 1986.

[13]Tuckness, D. G., and Jost, B., "A Critical Analysis of the Lunar Gravity Potential Model," *Journal of Spacecraft and Rockets* (accepted for publication).

[14]Aldrich, A., D., *The Space Exploration Initiative*, NASA Office of Aeronautics, Exploration, and Technology, Feb. 17, 1990, p. 4.

[15]Tuckness, D. G., "Future Lunar Landing Navigation Schemes with Emphasis on Precision Landings," *Journal of the Institute of Navigation*, Vol. 41, No. 2, 1994, pp. 215–288.

[16]Anon., "Status and Future of Lunar Geoscience," NASA SP-484, 1986.

[17]Cherry, G. W., "E Guidance—a General Explicit Optimizing Guidance Law for Rocket-Propelled Spacecraft," MIT Instrumentation Lab. TR R-456, 1964.

A. L. Vampola
Associate Editor